Mechanisms of crazing in glassy polymers revealed by molecular dynamics simulations

Dhiraj K. Mahajan* and Alexander Hartmaier

Interdisciplinary Centre for Advanced Materials Simulation, Ruhr-Universität Bochum, Stiepeler Strasse 129, Bochum 44801, Germany

(Received 23 March 2012; revised manuscript received 9 June 2012; published 10 August 2012)

Mechanisms leading to initiation of crazing type failure in a glassy polymer are not clearly understood. This is mainly due to the difficulty in characterizing the stress state and polymer configuration sufficiently locally at the craze initiation site. Using molecular dynamics simulations, we have now been able to access this information and have shown that the local heterogeneous deformation leads to craze initiation in glassy polymers. We found that zones of high plastic activity are constrained by their neighborhood and become unstable, initiating crazing from these sites. Furthermore, based on the constant flow stresses observed in the unstable zones, we conclude that microcavitation is the essential local deformation mode to trigger crazing in glassy polymers. Our results demonstrate the basic difference in the local deformation mode as well as the conditions that lead to either shear-yielding or crazing type failures in glassy polymers. We anticipate our paper to help in devising a new criterion for craze initiation that not only considers the stress state, but also considers local deformation heterogeneities that form the necessary condition for crazing in glassy polymers.

DOI: 10.1103/PhysRevE.86.021802 PACS number(s): 82.35.Lr, 83.50.−v, 81.05.Lg, 66.70.Hk

I. INTRODUCTION

Crazing and shear-yielding are two complementary types of failure of glassy polymers [1]. While the former leads to localization of deformation in the form of cavitation induced fibrillated zones, the latter causes concentrated deformation in shear zones with negligible volume change. In contrast to shear yielding [2,3], the atomic-scale mechanisms leading to the initiation of crazing are not clearly understood. Throughout the last four decades, continuous efforts have been conducted to identify the mechanisms of craze initiation and to establish a physics-based criterion. It started with a purely phenomenological model of a craze initiation criterion based on global shear stress [4], critical tensile strain [5], and a physically motivated criterion [6,7] that considers microcrack formation by the arrest of microshear bands around molecular heterogeneities. A recent refinement [8] of this model, based on developments borrowed from the mechanics of ductile fracture of metals, predicts the plastic expansion of nascent cavities due to the synergistic combination of local hydrostatic stresses and deviatoric shear stresses. Furthermore, a criterion based on linear elastic fracture mechanics [9] was proposed that considers craze initiation to be a frustrated fracture process rather than a yield mechanism. Clearly, no general agreement exists either on the understanding of the mechanisms or on the modeling of craze initiation, which is due to the difficulty in characterizing the stress state and polymer configuration sufficiently locally at the craze initiation site.

In this paper, we explore the conditions of craze initiation in comparison to shear-yielding using molecular dynamics (MD) simulations of a well equilibrated sample [10,11] of a glassy polymer. We perform deformation simulations using different multiaxial loading conditions that lead to crazing as well as shear-yielding type failure of the polymer sample. We will show that the global stress state of the MD sample describes the classical failure criteria for both types of failures. Additionally, the local failure conditions within the MD sample are obtained by monitoring the stress state and irreversible deformation of small volume elements during deformation. We found that the crazing initiates from the sites that show a large gradient of local irreversible deformation, supported by constant flow stress levels throughout the simulation box. We consider our findings to help framing a new criterion considering not only the stress state, but also the deformation heterogeneities essential for this mode of failure.

II. METHODS

We consider the united atom model of amorphous polyethylene, used in the paper of Bouvard *et al.* [12], as a model system for glassy polymers. The MD sample consists of 160 molecular chains of chain length 200 and is fully periodic in all directions. The initial sample is obtained at $T = 500$ K using a procedure outlined in a previous paper [11]. The sample dimensions provide sufficient molecular packing heterogeneities involved in the precursor process of crazing [13]. A glass transition temperature (T_g) of around 250 K is obtained by quenching the sample as an *NPT* ensemble from $T = 500$ to $T = 25$ K at a quench rate of $\dot{T} = 0.08$ K ps^{-1}. The conditions for crazing and shear-yielding type failures are generated by imposing multiaxial loading conditions on the quenched MD sample using different strain rates along the x, y, and z directions [14]. Multiaxial deformation simulations are performed at $T = 25$ K by imposing a constant true strain rate on the order of 10^8 s^{-1} in the direction of deformation as given in Table I. The time step adopted for deformation simulations is 1 fs. All calculations are performed using the molecular dynamics code LAMMPS [15].

For all loading cases, the global stress level is quantified in terms of deviatoric shear stress $\tau^{\text{dev}} = [\frac{1}{2}\text{Tr}(\boldsymbol{\sigma} - \sigma \boldsymbol{I})^2]^{1/2}$, where $\boldsymbol{\sigma}$ is virial stress tensor, $\sigma = (\sigma_{xx} + \sigma_{yy} + \sigma_{zz})/3$ is the hydrostatic stress, and $\boldsymbol{I}$ is the unit tensor. The deformation level is quantified in terms of a work conjugate definition of shear strain [13] $\varepsilon^{\text{dev}} = [2\text{Tr}(\boldsymbol{\varepsilon} - \frac{1}{3}\varepsilon \boldsymbol{I})^2]^{1/2}$, where $\boldsymbol{\varepsilon}$ is the true strain tensor and $\varepsilon = \varepsilon_{xx} + \varepsilon_{yy} + \varepsilon_{zz}$ is the volumetric strain. The initial sample after quenching has a value of $\tau^{\text{dev}} = 0$, hydrostatic pressure $(P) = 0$ and density $(\rho) = 920$ kg/m^3.

*dhiraj.mahajan@icams.rub.de

TABLE I. Summary of different multiaxial loading cases used in the present paper. The true strain rate employed along each direction is given by the numerical values in different columns. The dash symbol '–' represents the direction along which the pressure is kept at zero using *NPT* dynamics with temperature damping parameter $\tau_T = 5 \times 10^{-14}$s and pressure damping parameter $\tau_P = 5 \times 10^{-13}$ s.

Case	$\dot{\varepsilon}_{xx}(10^8\ \mathrm{s}^{-1})$	$\dot{\varepsilon}_{yy}(10^8\ \mathrm{s}^{-1})$	$\dot{\varepsilon}_{zz}(10^8\ \mathrm{s}^{-1})$
1	−1.0	–	–
2	1.0	−0.5	−0.5
3	2.2	−0.5	−1.25
4	1.0	–	–
5	1.0	1.0	–
6	2.5	−0.5	−1.0
7	1.0	1.0	−1.0
8	2.5	1.2	−1.7
9	−0.3	2.0	0.5
10	−0.8	1.0	2.0
11	0.5	1.5	−0.5
12	1.0	1.0	−0.5
13	−0.5	1.5	0.9
14	1.0	0.0	0.0
15	1.5	0.0	1.5
16	1.5	2.0	0.0
17	0.0	1.5	1.5

Additionally, to determine the local condition of failure, coarse graining of simulation quantities is performed from a single atom up to various length scales by subdividing the simulation cell into 27, 64, 125, 216, 343, and 1000 equal volume voxels containing, on average, 1185, 500, 256, 148, 93, and 32 united atoms, respectively. The atomic stress tensor is computed from the usual virial expression [13,16,17] in which the volume associated with each atom is obtained from Voronoi tessellation [18] of the simulation box. The virial stress tensor for voxels is computed as the weighted average of the atomic stresses for the atoms residing in voxels,

$$\boldsymbol{\sigma}^K = \frac{\sum_j \boldsymbol{\sigma}^j v^j}{\sum_j v^j},$$

where $\boldsymbol{\sigma}^j$ and v^j are the atomic stress tensor and atomic volume, respectively, for atom j that resides in the voxel K at a particular time [16]. This scheme leads to the evaluation of the global stress tensor when the simulation box is considered as a single voxel.

III. RESULTS

The stress strain behavior obtained during different multiaxial loading conditions is shown in Fig. 1(a). Failure in the MD sample is marked by a drop in the shear stress. Two groups of curves can be identified according to the failure stress. In the loading cases exhibiting lower failure stress, the sample fails by cavitation, leading to craze initiation in the MD sample. In contrast, no such cavitation is observed in the load cases with a higher failure stress, representing shear-yielding type failure.

In Fig. 1(b), the shear stress is plotted vs the hydrostatic pressure $(-\sigma)$ at yield. As can be seen, the data points are fitted

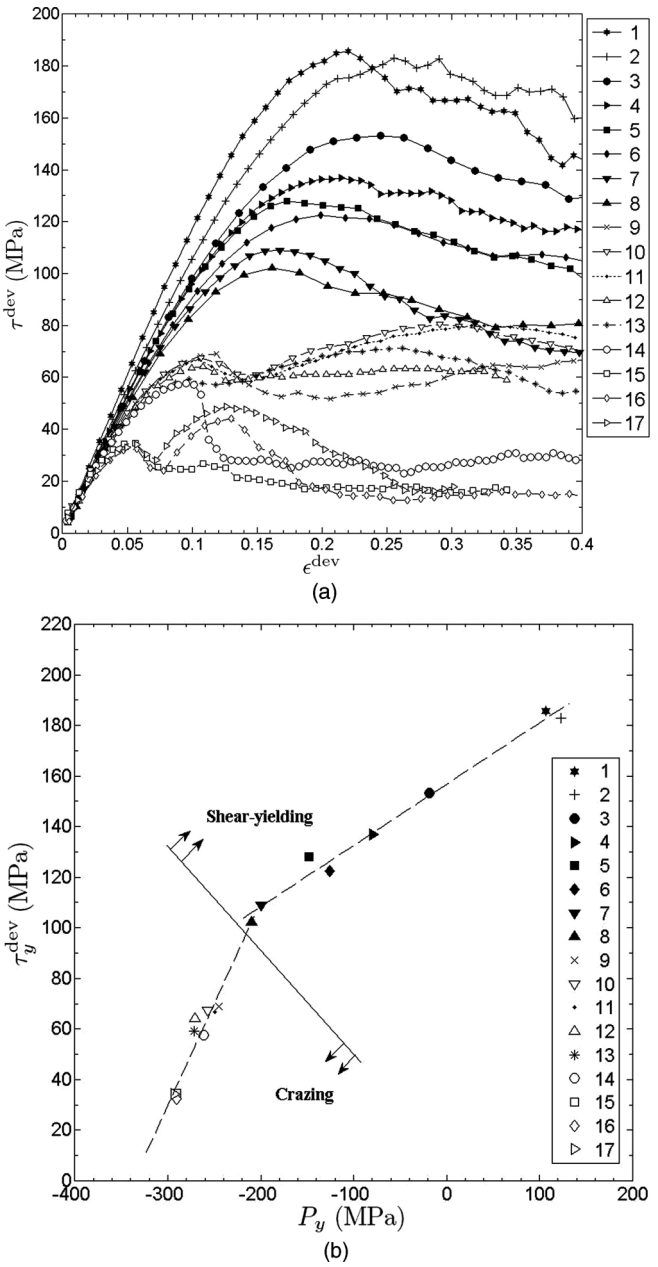

FIG. 1. Initially identical atomistic sample deformed under different multiaxial loading conditions as given in Table I for each loading case number marked by specific symbols. (a) The curves of deviatoric shear stress vs deviatoric shear strain can be grouped into two categories that correspond to either filled symbols: shear type failure or open symbols: crazing type failure as seen in (b) the plot of deviatoric shear stress at yield τ_y^{dev} vs hydrostatic pressure at yield P_y.

by two straight lines indicating different failure mechanisms for shear-yielding and crazing type failures. Data points referring to shear type failure are fitted using the pressure modified von Mises (pmvM) criterion,

$$\tau_y^{dev} = \tau_y^o + \alpha P_y, \quad (1)$$

where τ_y^{dev} is the deviatoric shear stress and P_y is hydrostatic pressure at yield, the coefficient τ_y^o depends on temperature, strain rate as well as the thermomechanical history of the polymer, and α is a dimensionless pressure coefficient. Data

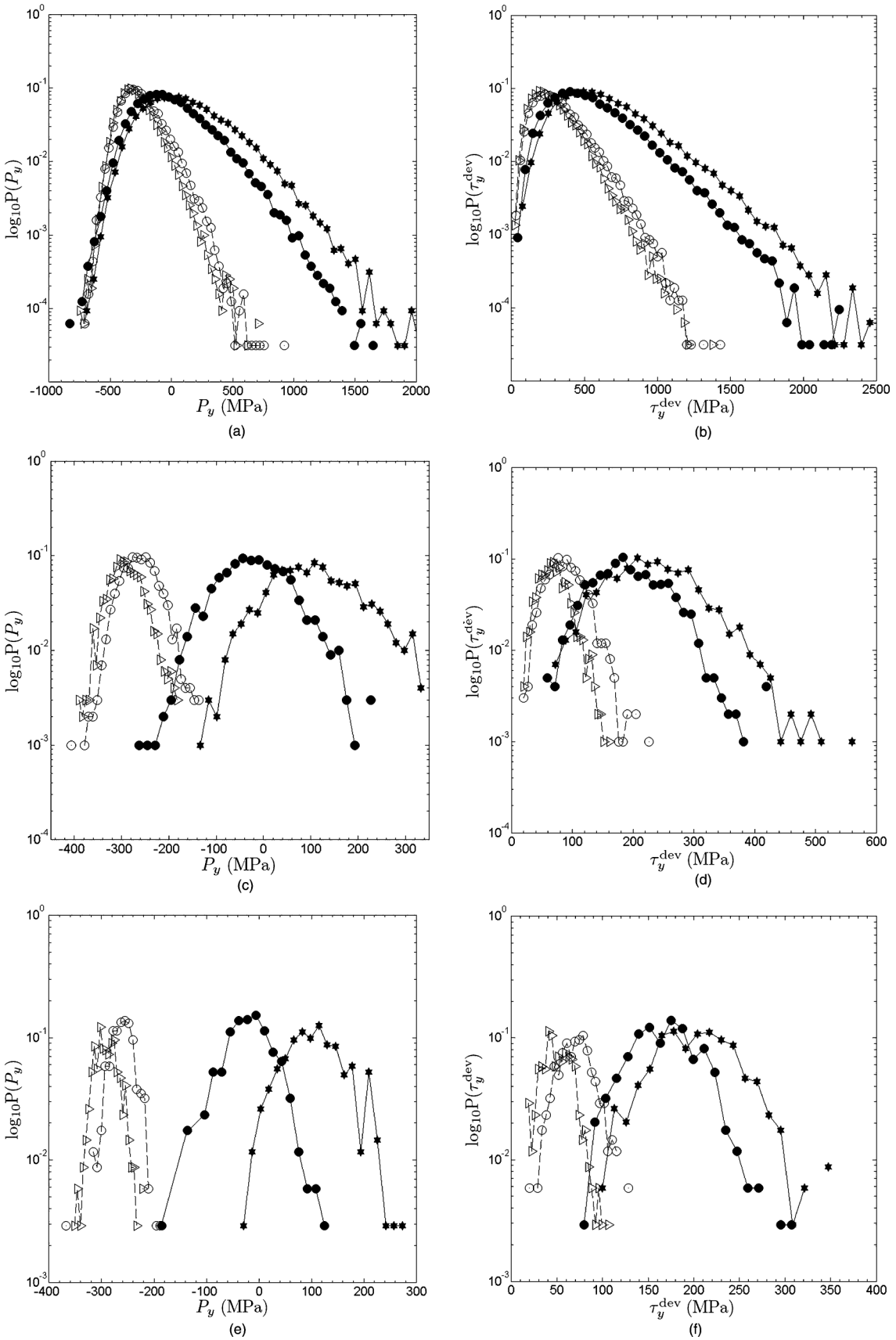

FIG. 2. Probability distribution of pressure and deviatoric shear stress at yield at the (a) and (b) atomic level as well as at the (c) and (d) coarse graining level with $\langle N^{\text{bin}} \rangle = 32$ and (e) and (f) $\langle N^{\text{bin}} \rangle = 93$, respectively. As in Fig. 1, open symbols used here represent crazing type failure, whereas, filled symbols represent shear-yielding type failure for the loading conditions as given in Table I.

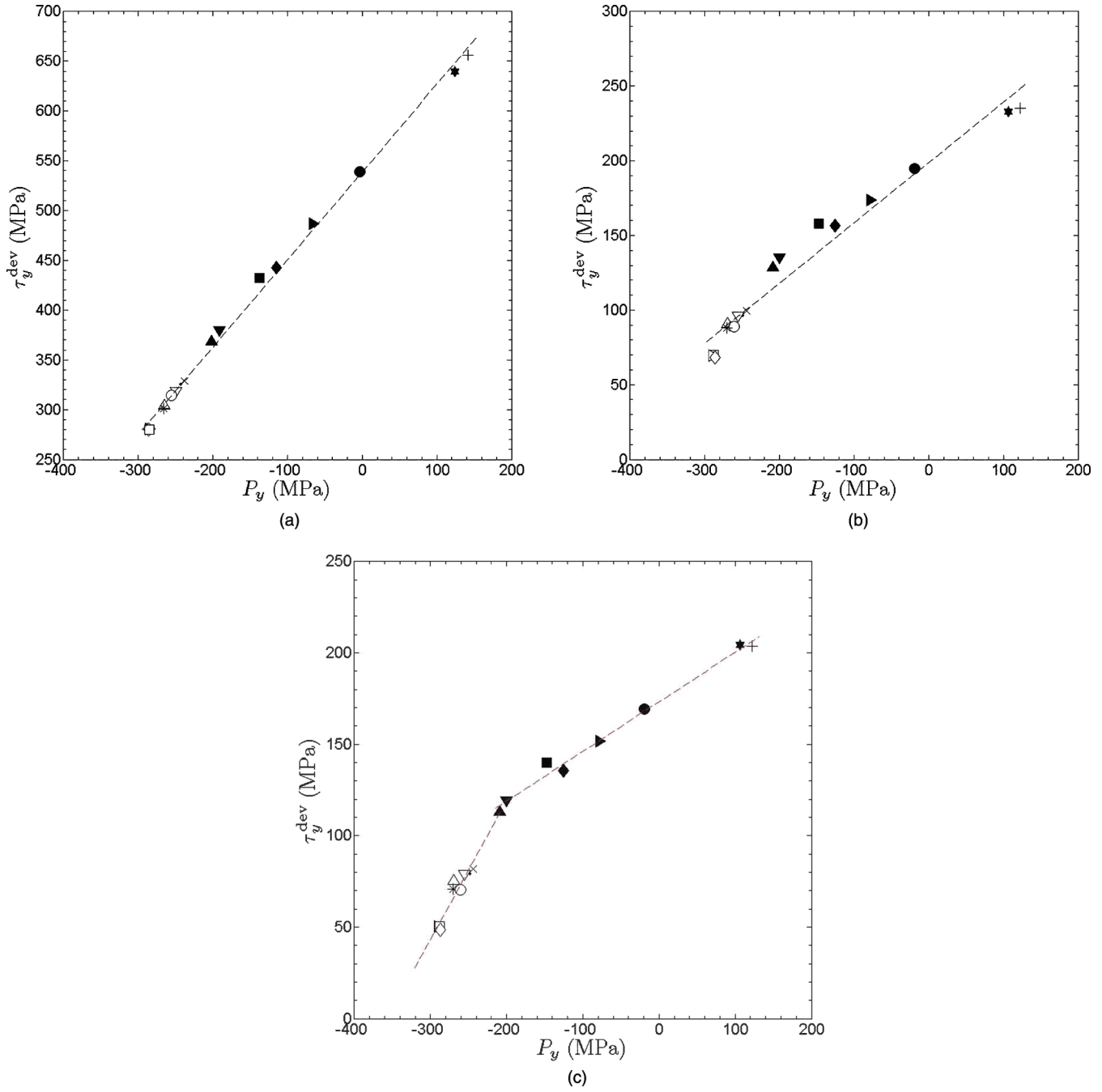

FIG. 3. (Color online) For different multiaxial loading cases at yield, the stress state at the (a) atomic level as well as at the (b) coarse graining level with $\langle N^{bin}\rangle = 32$ and (c) $\langle N^{bin}\rangle = 93$, respectively, is represented by the mean value of probability distribution of pressure and deviatoric shear stress, cf. Fig. 2. Symbols used here are the same as used in Fig. 1, corresponding to the specific loading case number given in Table I. All data points in (a) and (b) are fitted using pmvM criterion, whereas, in (c), the data corresponding to crazing and shear-yielding type failures can only be fitted seperately by their respective criterion. Fitting coefficients for the failure criteria at all levels of coarse graining are given in Table III.

points representing crazing type failure are fitted separately using Sternstein's craze initiation criterion [4,19], expressed in terms of deviatoric shear stress and pressure at yield as

$$\tau_y^{dev} = A - \frac{B}{P_y}, \tag{2}$$

where A and B are temperature dependent coefficients. The inverse relation of deviatoric shear stress with pressure together with a negative and a positive value obtained for constants A and B during experiments [4] confirms the absence of crazing under a pure shear and compressive stress state (positive hydrostatic pressure). The value obtained for different constants from fitting is given in Table II, which is consistent with experiments [1,4,20,21] as well as other simulation papers [19,22] performed using the bead-spring model of glassy polymers. However, having used a detailed model of glassy

TABLE II. Values of coefficients characterizing the global shear-yielding and craze initiation criteria.

pmvM criterion		Sternstein craze initiation criterion	
τ_y^o (MPa)	α	A (MPa)	B (MPa)^2
156	0.24	−139	51 582

polymers consisting of angular and dihedral interactions, the value obtained for different constants matches more closely with the experimental value in comparison to the one obtained by using the bead-spring model. From these results, it becomes evident that the global stress state of the MD sample is well described by classical failure criteria for both types of failure. Hence, we can employ our MD simulations to find the local conditions that lead to craze initiation (cavitation) at specific sites.

A. Local failure behavior

The local failure conditions can be evaluated by tracking properties of a subset of atoms corresponding to different levels of coarse graining. The scale up to which the global failure behavior correlates with the local stress state is obtained by binning the simulation box into equal size voxels and evaluating their stress state at the yield point, similar to the paper of Macneill and Rottler [16]. For all multiaxial loading cases as well as at different levels of coarse graining, the local stress state at yield is obtained from the probability distribution of pressure and deviatoric shear stress in voxels. The mean value of these distributions is used to fit the failure criterion at various levels of coarse graining, starting from a single atom to bins with average atoms per bin ($\langle N^{\text{bin}}\rangle$) equal to 32, 93, 148, 256, 500, and 1185.

Figures 2(a) and 2(b) show the atomic level probability distributions of pressure and deviatoric shear stress, respectively, at the yield point for two cases each of crazing and shear-yielding type failure. Similar distributions corresponding to the coarse graining level with $\langle N^{\text{bin}}\rangle = 32$ and 93 are shown in Figs. 2(c)–2(f), respectively. At all levels of coarse graining, we see that the stress distributions for crazing type failure are much narrower than the distributions corresponding to shear-yielding type failure. Furthermore, with the increasing level of coarse graining, the stress distributions become narrower in general.

Subsequently, the mean values of pressure and deviatoric shear stress distributions are used to obtain the failure criterion at different levels of coarse graining. Figure 3(a) shows the stress state at the yield point at the atomic level for different multiaxial loading conditions. The stress states for the coarse graining level with $\langle N^{\text{bin}}\rangle = 32$ and 93 are shown in Figs. 3(b) and 3(c), respectively. We see that all data points, representing the stress state at the atomic level, Fig. 3(a), and for coarse graining level with $\langle N^{\text{bin}}\rangle = 32$, Fig. 3(b), fall on a straight line and are fitted using the pmvM criterion. However, the stress state for bins with $\langle N^{\text{bin}}\rangle = 93$ or higher correlates with the global failure behavior such that the data points corresponding to crazing and shear-yielding type failures can only be fitted by separate failure criteria. Hence, the bin size corresponding to $\langle N^{\text{bin}}\rangle = 93$ has been used as the smallest length scale to represent the local conditions of failure. The values obtained for the failure criterion coefficient at different levels of coarse graining are given in Table III. We see that values of these coefficients start converging sharply with the global values for the coarse graining level with $\langle N^{\text{bin}}\rangle = 93$ and onwards. A similar result is obtained with respect to the level of coarse graining that correlates with the global failure criterion by using the bead-spring model of a glassy polymer [16].

TABLE III. Values of coefficients characterizing the local shear-yielding and craze initiation criterion at different levels of coarse graining.

Atoms/bin	pmvM criterion		Sternstein craze initiation criterion	
$\langle N^{\text{bin}}\rangle$	τ_y^o (MPa)	α	A (MPa)	B (MPa)^2
1185	158	0.24	−140	51 640
256	162	0.25	−131	50 307
148	167	0.26	−125	49 577
93	173	0.27	−114	48 200
32	199	0.4		
1	539	0.88		

B. Mechanisms of craze initiation

At the local scale, the glassy polymer structure is characterized by both dynamical [23] and mechanical heterogeneities [24]. In recent papers [25,26], it was shown that mechanical heterogeneities in the form of weak elastic zones act as favorite spots of cavity formation. However, a fundamental understanding of the mechanisms leading to craze initiation is

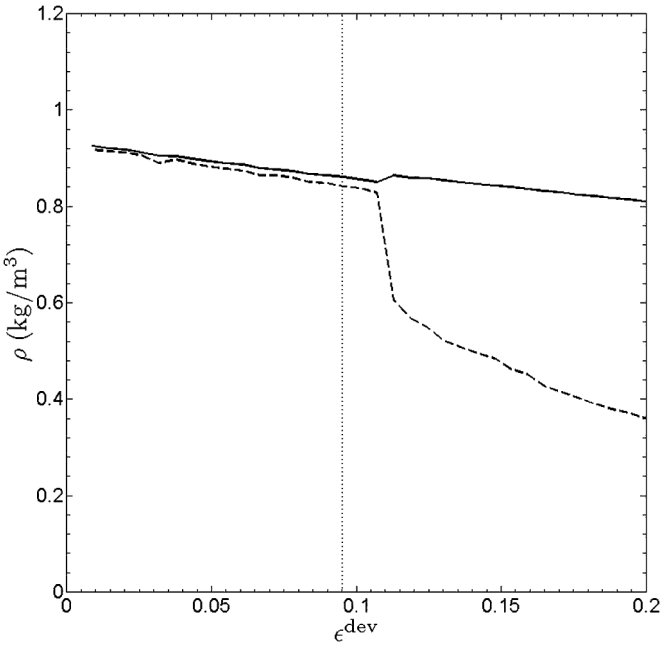

FIG. 4. Dashed line: average density in craze initiation bins in comparison to the solid line: average density of all other bins not involved in crazing as a function of deviatoric shear strain. The macroscopic yield strain is marked by a vertical dotted line.

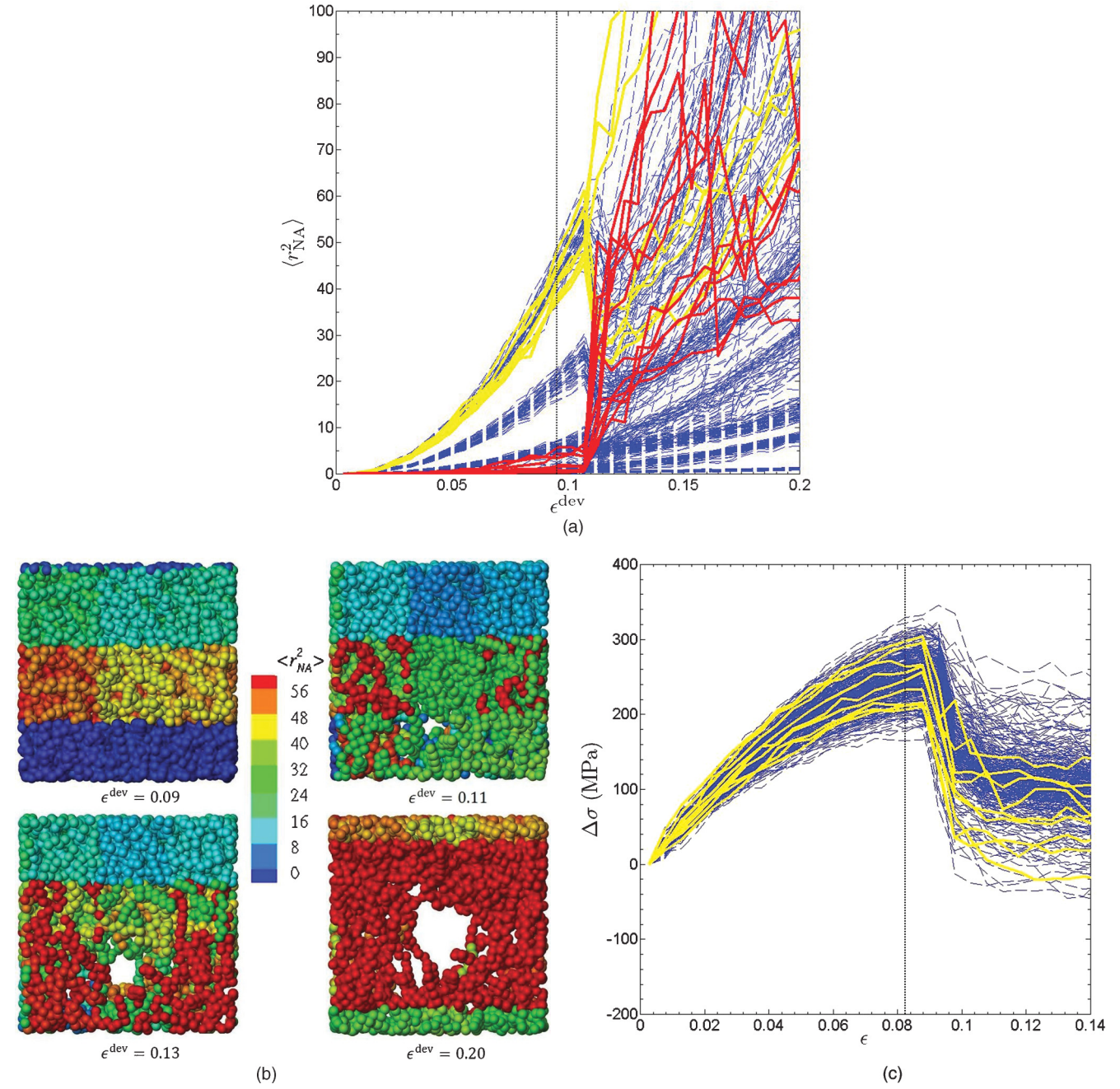

FIG. 5. (Color online) (a) Deformation during crazing type failure is highly heterogeneous as shown in the plot of average irreversible deformations $\langle r^2_{\mathrm{NA}} \rangle$ in different bins vs global deviatoric shear strain $\varepsilon^{\mathrm{dev}}$. Craze initiation bins are marked by yellow and red curves and show contrasting behavior with respect to irreversible deformations. Bins that are not involved in crazing are marked by blue curves. The macroscopic yield strain is marked by a vertical dotted line. (b) The atomic configuration of the craze initiation bins with respect to $\langle r^2_{\mathrm{NA}} \rangle$ values is shown at $\varepsilon^{\mathrm{dev}} = 0.09, 0.11, 0.13,$ and 0.2. The color scheme used for atoms represents the average irreversible deformation in different bins. (c) The evolution of hydrostatic stress $\Delta\sigma$ in different bins vs global volumetric strain εconfirms that high plastic activity crazing bins (shown as yellow curves) are among the first few bins that become unstable close to the macroscopic yield, thus, initiating crazing from these locations.

expected to result from a detailed analysis of the dynamic heterogeneities. In this paper, the heterogeneous dynamics of the deforming system is characterized by nonaffine displacements [27]. Nonaffine displacements for each atom are calculated using a standard definition [16] as $\boldsymbol{r}_{\mathrm{NA}} = \boldsymbol{r}_t - \boldsymbol{r}_{t_o} - \boldsymbol{\varepsilon}\boldsymbol{r}_{t_o}$, where $\boldsymbol{\varepsilon}$ is the global strain tensor and $\boldsymbol{r}_{t_o}$ and $\boldsymbol{r}_t$are the atomic position vectors at initial time t_o and current time t. A scalar form of nonaffine displacements $r^2_{\mathrm{NA}} (= \boldsymbol{r}_{\mathrm{NA}} \cdot \boldsymbol{r}_{\mathrm{NA}})$ is associated with all atoms as the measure of local irreversible deformation.

To characterize local conditions of craze initiation and its fundamental difference with shear-yielding type failure, we analyze two loading cases closely: one with strain rate $\dot{\varepsilon}_{xx} = 1, \dot{\varepsilon}_{yy} = 0,$ and $\dot{\varepsilon}_{zz} = 0$ [10^8 s^{-1}] leading to crazing type

failure and another with strain rate $\dot{\varepsilon}_{xx} - 2.2, \dot{\varepsilon}_{yy} = 0.5$, and $\dot{\varepsilon}_{zz} = -1.25$ [10^8 s^{-1}] causing shear yielding. In Fig. 1(a), the stress strain behavior for the former and the latter case is marked by curves with filled circle and open circle symbols, respectively. During crazing type failure, a sharp drop in shear stress level marks cavitation of the MD sample that initiates crazing. The location of craze initiation in the MD sample is detected in those bins that showed a sharp decrease in density ($\rho < 700\,kg/m^3$) in comparison to the average density ($\rho \approx 900\,kg/m^3$) of all other bins at the yield point. The variation in average density in craze initiation bins and all other bins not involved in crazing is shown in Fig. 4 as a function of deviatoric shear strain. The macroscopic yield strain, after which the crazing is initiated, is marked by a vertical dotted line. In total, 25 craze initiation bins are identified that lie in close proximity to each other within the MD sample.

Figure 5(a) shows the evolution of average irreversible deformation ($\langle r^2_{NA}\rangle = \sum_1^{N^{bin}} r^2_{NA}/N^{bin}$) in different bins during crazing type failure. Deformation during crazing type failure is highly heterogeneous, and the onset of crazing leads to instability as observed by a sharp fluctuation in $\langle r^2_{NA}\rangle$ values for most of the bins. Bins involved in craze initiation (as explained before) show contrasting behavior with respect to irreversible deformation. Although a few of the crazing bins show high levels of plastic activity (yellow curves) before cavitation, the rest of the crazing bins exhibit low levels of plastic activity (red curves) as seen in Fig. 5(a). Atomic configurations of bins in the vicinity of the location of craze initiation at macroscopic yield and after cavitation are shown in Fig. 5(b). Atoms in different bins are colored according to the average irreversible deformation values ($\langle r^2_{NA}\rangle$) for these bins. It appears that deformation in high plastic activity crazing bins is constrained by low plastic activity crazing bins that lie in their neighborhood. Figure 5(c) shows the evolution of hydrostatic stress $\Delta\sigma = \sigma(t) - \sigma(t_o = 0)$ with volumetric strain (ε), and for different bins, the behavior of high plastic activity crazing bins is shown as yellow curves. It is seen that few of these bins are among the first bins that become unstable causing instantaneous growth of voids from these bins that also expands into the neighboring crazing bins that showed low levels of plastic activity before cavitation. The conditions shown for craze initiation are similar

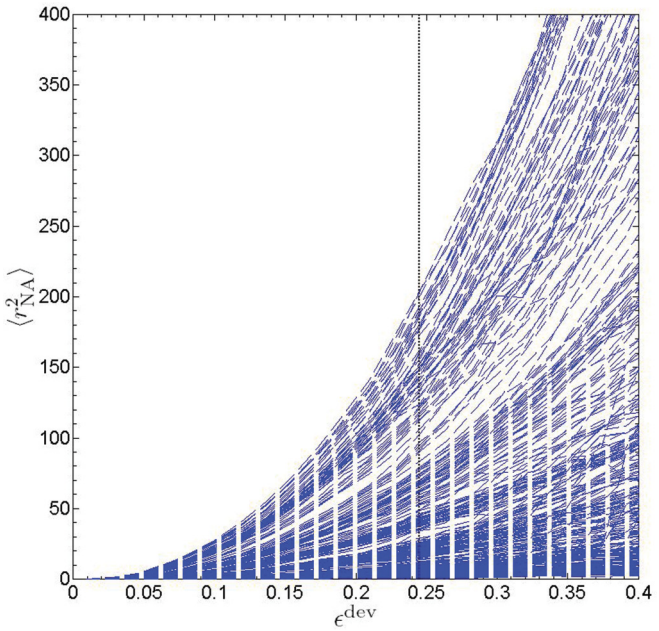

FIG. 6. (Color online) Variation in average irreversible deformations $\langle r^2_{NA}\rangle$ in different bins vs global deviatoric shear strain ε^{dev} during shear-yielding type failure. The macroscopic yield strain is marked by the vertical dotted line.

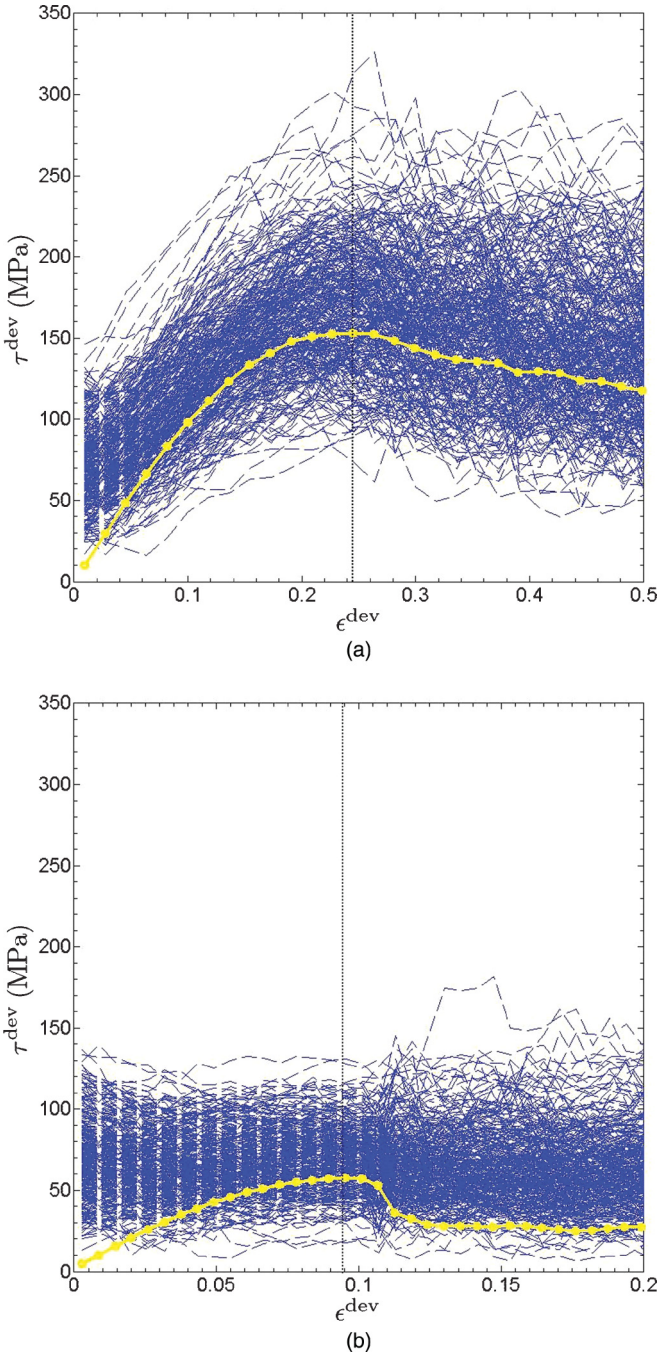

FIG. 7. (Color online) (a) Bin level deviatoric shear stress vs global deviatoric strain for the loading case that leads to shear-yielding type failure and (b) crazing type failure. Global deviatoric stress variation is shown as the dotted yellow curve for both cases, and macroscopic yield is marked by a vertical dotted line.

to cavitation instabilities observed in ductile metals under highly constrained plastic flow [28]. In contrast, irreversible deformation during shear-yielding type failure spreads more homogeneously throughout the MD sample (cf. Fig. 6) and does not show any instability as observed during crazing type failure. This difference in behavior can be linked to the characteristics of local deformation, which, in turn, can be interpreted from the evolution of bin level shear stresses with global deformation.

Figure 7(a) shows the evolution of bin level shear stress (τ^{dev}) with global shear strain (ε^{dev}) for shear-yielding type failure. Global shear flow stress evolution is shown as a dotted yellow curve. Different initial stress levels for different bins confirm mechanical heterogeneities. Furthermore, it is understood that global shear flow stress cannot be an average value of bin level shear flow stresses as, even though the MD sample is equilibrated to zero pressure before deformation, the residual (misfit) stresses in the bins remain nonzero, which is a characteristic property of an amorphous system. A monotonous increase in shear flow stress for most of the bins confirms local conformational modifications of polymer chains with deformation. The changing molecular conformation will gradually enforce the conformational changes in the neighboring molecules leading to more homogenous deformation and giving rise to increasing shear stresses throughout the MD sample before macroscopic yielding. The macroscopic yield point for shear-yielding type failure exerts a limit to such deformations after which the material starts to flow at constant stress levels due to increased local volume resulting from conformation changes in molecules. Figure 7(b) shows the variation of bin level shear flow stress for crazing type failure. Global shear flow stress evolution is shown as a dotted yellow curve. Almost constant flow stress levels in different bins during deformation suggest little or no conformational change [13] of polymer chains but a sharp increase in the initial porosity throughout the MD system as also suggested by increasing hydrostatic stress [cf. Fig. 5(c)] for all bins. This mode of deformation can be highly heterogeneous as it does not demand the modification of neighboring chains conformation. However, a limit is placed on the highly cavitating zones by the neighboring zones that are not cavitating at the same intensity [cf. Fig. 5(a)]. This causes instabilities in former zones and leads to craze initiation from these zones.

IV. SUMMARY AND DISCUSSION

In this paper, we examined the conditions for crazing and shear-yielding type failures of glassy polymers using MD simulations. We see that the experimental failure criteria are followed for the global failure behavior of the MD sample. By partitioning the simulation cell into voxels at different length scales and using the probability distributions of stress levels in voxels, we found that the local failure conditions correlate with the global failure conditions for voxels containing an average atom as around 90 and above. Subsequently, the local conditions in terms of stress levels and irreversible deformations are tracked at this length scale to reveal the mechanism of craze initiation in the simulation box.

We see that the crazing initiates at the sites that show the highest gradient in local irreversible deformations within the simulation box, showing explicitly the role of heterogeneities in initiating this mode of failure. For crazing, microcavitation is the local mode of deformation of the polymer sample as supported by the observation of constant local flow stress levels. On the other hand, for shear-yielding type failure, the local deformation causes conformational changes in polymer chains as supported by the observation of increasing flow stress level throughout the simulation box up to the yield point.

Insight provided by the detailed MD simulations of a glassy polymer on the craze initiation explains the behavior of the crazing process that is mainly a surface phenomenon or initiates at the intersection of shear bands in front of crack tips under plane strain conditions. These locations show large deformation inhomogeneities and, thus, are favorable sites for crazing. The findings from this paper have provided new insight into craze initiation mechanisms that will help framing a new criterion considering not only the stress state, but also the deformation inhomogeneities essential for this mode of failure.

ACKNOWLEDGMENTS

The authors acknowledge financial support through ThyssenKrupp AG, Bayer MaterialScience AG, Salzgitter Mannesmann Forschung GmbH, Robert Bosch GmbH, Benteler Stahl/Rohr GmbH, Bayer Technology ServicesGmbH, the state of North-Rhine Westphalia, as well as the EU in the framework of the ERDF.

[1] R. N. Haward and R. J. Young, *The Physics of Glassy Polymers* (Chapman & Hall, London, 1997).
[2] A. S. Argon, Philos. Mag. **28**, 839 (1973).
[3] N. Brown, J. Mater. Sci. **48**, 2241 (1983).
[4] S. S. Sternstein and F. A. Myers, J. Macromol. Sci., Phys. B **8**, 539 (1973).
[5] R. J. Oxborough and P. B. Bowden, Philos. Mag. **28**, 547 (1973).
[6] A. S. Argon, J. Macromol. Sci., Phys. B **8**, 573 (1973).
[7] A. S. Argon and J. G. Hannoosh, Philos. Mag. **36**, 1195 (1977).
[8] A. S. Argon, Polymer **52**, 2319 (2011).
[9] C. B. Bucknall, Polymer **48**, 1030 (2007).
[10] D. K. Mahajan and S. Basu, Int. J. App. Mech. **2**, 515 (2010).
[11] D. K. Mahajan and S. Basu, Modell. Simul. Mater. Sci. Eng. **18**, 025001 (2010).
[12] J. L. Bouvard *et al.*, Acta Mech. **213**, 71 (2010).
[13] P. H. Mott, A. S. Argon, and U. H. Suter, Philos. Mag. A **68**, 537 (1993).
[14] J. Rottler and M. O. Robbins, Phys. Rev. E **68**, 011801 (2003).
[15] S. Plimpton, J. Comput. Phys. **117**, 1 (1995).
[16] D. MacNeill and J. Rottler, Phys. Rev. E **81**, 011804 (2010).
[17] D. K. Mahajan, B. Singh, and S. Basu, Phys. Rev. E **82**, 011803 (2010).
[18] http://math.lbl.gov/voro++/.

[19] R. Estevez and D. Long, Modell. Simul. Mater. Sci. Eng. **19**, 045004 (2011).
[20] P. B. Bowden and J. A. Jukes, J. Mater. Sci. **7**, 52 (1972).
[21] R. Quinson *et al*., J. Mater. Sci. **32**, 1371 (1997).
[22] J. Rottler and M. O. Robbins, Phys. Rev. E **64**, 051801 (2001).
[23] M. D. Ediger, Annu. Rev. Phys. Chem. **51**, 99 (2000).
[24] K. Yoshimoto, T. S. Jain, K. Van Workum, P. F. Nealey, and J. J. de Pablo, Phys. Rev. Lett. **93**, 175501 (2004).
[25] A. Makke, M. Perez, R. Rottler, O. Lame, and J. L. Barrat, Macromol. Theory Simul. **20**, 826 (2011).
[26] G. N. Toepperwein and J. J. de Pablo, Macromolecules **44**, 5498 (2011).
[27] R. A. Riggleman, H. N. Lee, M. D. Ediger, and J. J. de Pablo, Soft Matter **6**, 287 (2009).
[28] Y. Huang, J. W. Hutchinson, and V. Tvergaard, J. Mech. Phys. Solids **39**, 223 (1991).